Chemical bonding, electronic, and magnetic properties of $R_3Co_4Sn_{13}$ intermetallics (R=La, Ce, Sm, Gd, and Tb): Density functional calculations

Guohua Zhong,* Xiaowu Lei, and Jianggao Mao†

State Key Laboratory of Structural Chemistry, Fujian Institute of Research on the Structure of Matter, Chinese Academy of Sciences, Fuzhou, Fujian 350002, People's Republic of China

(Received 16 October 2008; revised manuscript received 9 February 2009; published 25 March 2009)

The structural, electronic, and magnetic properties in the intermetallic compounds, $R_3Co_4Sn_{13}$ (R=La, Ce, Sm, Gd, and Tb), have been investigated by performing density functional theory (DFT) and DFT+U calculations. The stability, bonding character, charge density, total and partial density of states, and band structure, as well as Fermi-surface feature, were analyzed. In particular, we clearly present the 4f electronic characters in these series. The antibonding states formed by Co 3d and Sn 5p play an important role in the superconductivity of $La_3Co_4Sn_{13}$. 4f electrons exhibit itinerancy and strongly couple with conduction electron, and these properties show strong dependence on the U parameter in the Ce compound. On the contrary, 4f electrons are fully localized at the deep energy level, and their energies do not change with the U parameter in the Gd compound. In Sm and Tb compounds, localization and itinerancy of 4f electrons coexist. In these compounds, magnetism mainly results from 4f electrons, while Co and Sn atoms hardly contribute a magnetic moment because of their sublattice structure and covalent interaction. Comparably, La compound is a nonmagnetic superconductor with the competition between superconductivity and magnetism. $Ce_3Co_4Sn_{13}$ is a weak itinerant ferromagnetic metal with a semimetallic behavior. The antiferromagnetic ordering exists in Gd compound. Both $Sm_3Co_4Sn_{13}$ and $Tb_3Co_4Sn_{13}$ are ferromagnetic metals. The trivalent charge state of rare-earth ions is suggested in these compounds.

DOI: 10.1103/PhysRevB.79.094424 PACS number(s): 75.20.En, 71.20.Eh, 71.20.Lp, 71.20.Ps

I. INTRODUCTION

R-TM-Sn (R represents rare-earth element and TM represents transition metal) intermetallic compounds have attracted much attention due to the interesting properties such as Kondo effect, mixed-valence phenomenon, heavy fermion behavior, superconductivity, and complicated magnetism.[1,2] The study of R-TM-Sn ternary stannides is helpful in understanding the nature of d and f electrons, especially for f electrons. Numerous experimental works have been reported. The heavy fermion behavior with larger electronic specific-heat coefficient γ was found in CeNiSn,[3] YbRhSn [$\gamma \sim 1200$ mJ/(mol K^2)],[4–8] and $Ce_3TM_4Sn_{13}$ [TM=Ir,[9–11] Pt,[12] and Co (Refs. 13–16)]. The Kondo effect was observed in CeRhSn (Ref. 17) and $Ce_3Co_4Sn_{13}$.[13–16] Moreover the superconductivity exists in LaRhSn ($T_c \sim 1.7$ K),[18] $Yb_3Rh_4Sn_{13}$ ($T_c \sim 8$ K),[19,20] and $La_3Co_4Sn_{13}$ ($T_c \sim 2.4$ or 2.85 K).[13,14] In addition, both CeNiSn (Ref. 3) and CeRhSn (Ref. 17) exhibit valence fluctuations phenomenon. The valence state of Eu^{2+} was demonstrated in $Eu_3Ir_4Sn_{13}$.[21] For R-TM-Sn systems, the variety of valence states indicates rich electronic and magnetic properties.

Interestingly, the R-TM-Sn compounds possess complicated magnetic structures because the open-shelled d and f electrons synchronously exist in these systems. Via the study on the magnetism of TM, it was found that the TM atoms had the considerable magnetic moments in the TM-rich systems, such as $La_6Co_{13}Sn$ (Ref. 22) and RCo_3Sn (R=Y and Gd-Yb).[23] In the equiatomic RRhSn and RNiSn group of compounds, however, the TM contribution to magnetism is negligible.[3–8,17,18,24,25] Meanwhile, the magnetic moment of Co atoms was not obviously observed in the tin-rich $R_3Co_4Sn_{13}$ (R=La-Nd, Sm, Gd, and Tb).[13–16,26–28] As a result, the magnetism is mainly induced by R atoms in most R-TM-Sn systems. From the magnetism of R atoms, the equiatomic CeNiSn and PrNiSn (Ref. 8) do not display magnetic order, and LaNiSn is a nonmagnetic (NM) compound, while NdNiSn is antiferromagnetic (AFM) below 2.8 K.[24,25] For the tin-rich $Yb_3Rh_4Sn_{13}$-type intermetallics, magnetism, and superconductivity coexist in $Yb_3Rh_4Sn_{13}$,[19,20] while $La_3Co_4Sn_{13}$ is a NM superconductor.[13,14] Compared to $Ce_3Ir_4Sn_{13}$ with the AFM ordering at 0.6 K, the magnetism of $Ce_3Co_4Sn_{13}$ is complex and disputed. Christianson *et al.*[16] suggested the possibility of AFM order in $Ce_3Co_4Sn_{13}$ since the neutron-diffraction data did not show any sign of magnetic scattering below 0.8 K. But magnetization data at 0.1 T showed a paramagnetic behavior down to 1.8 K for $Ce_3Co_4Sn_{13}$, with the effective magnetic moment of $2.56\mu_B/Ce^{3+}$ at room temperature.[14] Moreover, Cornelius *et al.*[15] did not observe the long-range magnetic order down to 0.35 K in zero field or obvious non-Fermi-liquid behavior. However, $Ce_3Co_4Sn_{13}$ is near the magnetic quantum critical point (QCP).[13–16] A possible magnetic phase transition occurs at a much lower temperature.[14,15] The electronic specific-heat coefficient of $Ce_3Co_4Sn_{13}$ increases dramatically due to magnetic short-range fluctuations, reaching a very large maximum value of $\sim$4280 mJ/(mol K^2) around the transition temperature from 75 mJ/(mol K^2) at zero temperature.[14] For Gd compounds, $Gd_3Co_4Sn_{13}$ is AFM order at low temperature (below 14.5 K) but paramagnetic metal at high temperature.[27] The magnetic transition exists in $Gd_3Ir_4Sn_{13}$ at 10 K too.[29] In addition, Pr, Nd, Sm, and Tb analogs have also been fabricated and characterized, but the study of physical properties is still lacking.

Analyzing experimental investigations above, it is worthy to note that these interesting physical properties mainly re-

sult from the 4*f* electrons whose theoretical research is still a challenge due to the more local and complicated features than 3*d* electrons. It is just the multiformity of *f* electronic structures that brings in the complicated magnetism. Aburto and Orgaz[30] theoretically studied the equiatomic *R*NiSn (*R* =La, Ce, Pr, and Nd) intermetallics as well as their hydrides. Comparing with the research efforts at experiments, however, the theoretical work is still inadequate to explore the nature of *f* electrons in *R*-TM-Sn intermetallic compounds. For 4*f* electronic characters such as localization or itinerancy, hybridization with conduction electron (c-e), correlation strength, and magnetic interaction as well as the competition between Ruderman-Kittel-Kasuya-Yosida (RKKY) and Kondo effect, much deeper theoretical understanding is needed. Noticeably, there is no 4*f* occupancy in La atom, there are only one-filled 4*f* electron in Ce atom and half-filled 4*f* occupancy in Gd atom with less than and more than half-filled cases in Sm and Tb atoms, respectively. Therefore, we present our results on the systematic investigation of crystal, electronic, and magnetic structures of $R_3Co_4Sn_{13}$ (*R*=La, Ce, Sm, Gd, and Tb) and also compare it with other *R*-TM-Sn systems in this work. Apart from another crystal structure, the study on this series of intermetallics is a better fundamental knowledge of bonding character, electronic structures, physical, and chemical properties of the *R*-TM-Sn-type intermetallics. It is an essential step toward their fascinating physical and chemical potentials.

II. STRUCTURAL MODEL AND COMPUTATIONAL METHOD

A. Structure

$R_3Co_4Sn_{13}$ (*R*=La, Ce, Sm, Gd, and Tb) crystallize in the $Pm\bar{3}n$ space group (No. 223) with the $Yb_3Rh_4Sn_{13}$ structure type.[19] Sn1, *R*, Co, and Sn2 atoms occupy the 2*a*, 6*d*, 8*e*, and 24*k* sites, respectively. The unit cell contains two formulas of $R_3Co_4Sn_{13}$ in these intermetallics, as shown in Fig. 1. The structure is similar to the $A'A''_3B_4O_{12}$-type ($Im\bar{3}$, No. 204) compounds such as $ACu_3Ti_4O_{12}$ (Ref. 31) and $CaCu_3Cr_4O_{12}$ (Ref. 32) where the *A* is replaced by *R* atoms. The Sn1 atoms occupy the origin of the unit cell and form an infinite network of edge-sharing $(Sn1)(Sn2)_{12}$ icosahedra. In spite of forming $R(Sn2)_{12}$ face-sharing and edge-sharing cuboctahedra, the *R* atoms seem to be isolated. The Co atoms form the $Co(Sn2)_6$ trigonal prisms which are corner sharing with a titled three-dimensional (3D) arrangement. These trigonal prisms encompass these Sn1 atoms. The feature of $Co(Sn2)_6$ is similar to the BO_6 octahedra in $A'A''_3B_4O_{12}$-type compounds. Additionally, $R_3Co_4Sn_{13}$ can also be regarded as the sum of two interpenetrating structures of R_3Sn and $CoSn_3$.[14]

B. Methodology

In this present work, the calculations of both crystal optimization and electronic structures were performed in the WIEN2K package.[33] The Kohn-Sham equations were solved by using the highly accurate all-electron full-potential linearized augmented plane-wave (FPLAPW) method[34,35] in the framework of density functional theory (DFT) with the exchange-correlation functional treated in the generalized gradient approximations (GGAs) of Wu-Cohen (WC) version.[36] This method makes no shape approximation to the potential or the electron density. Within the FPLAPW method, the unit cell is divided into nonoverlapping muffin-tin (MT) spheres and an interstitial region. Inside the muffin-tin sphere of radius R_{MT}, the wave functions are expanded using radial functions (solution to the radial Schrödinger equation) times spherical harmonics up to l_{max}^{wf}, and the expansion of the potential inside the muffin-tin spheres is carried out up to l_{max}^{pot}. The parameter $R_{MT}^{min} \times K_{max}$ (R_{MT}^{min} is the smallest muffin-tin spherical radius present in the system and K_{max} is the truncation of the modulus of the reciprocal-lattice vector) is used to determine the number of plane waves needed for the expansion of the wave function in the interstitial region, while the parameter G_{max} is used to truncate the plane-wave expansion of the potential and density in the interstitial region. Here, the MT radii were set to 2.3, 2.2, and 2.0 a.u. for the *R*, Co, and Sn atoms, respectively. Moreover, we let $R_{MT}^{min}K_{max}=7.0$, $l_{max}^{wf}=10$, $l_{max}^{pot}=4$, and $G_{max}=12$. The separate energy of −8.0 Ry was used between valence and core states. Thus, the *R* 4*f*5*d*6*s*, Co 3*d*4*s*, and Sn 5*s*5*p* were treated as valence states, while *R* 4*d*5*s*5*p*, Co 3*s*3*p*, and Sn 4*p*4*d* were acted as semicore states with other electrons as core states. The energy level of unoccupied states was calculated until 7.5 Ry ($E_{max}=7.5$ Ry). Integrations in the first Brillouin zone (FBZ) have been performed using the standard tetrahedron-method[37] with 4×4×4 Monkhorst-Pack special *k* points.[38] Self-consistency calculation of electronic structures is achieved when the total-energy variation from iteration to iteration converged to a 0.01 mRy accuracy or better.

In the WIEN2K code, core states were treated at the fully relativistic approximation while semicore and valence states were treated at the scalar relativistic level. Specifically, we adopted the second variational method[39] to consider the spin-

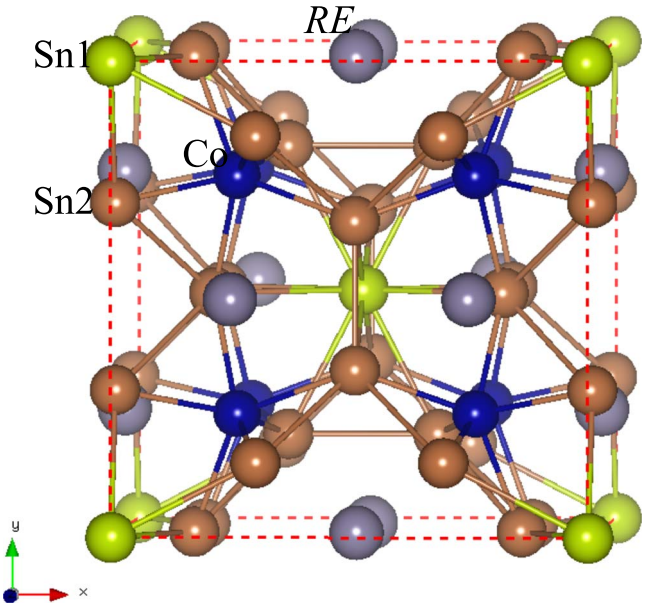

FIG. 1. (Color online) The unit-cell structure of $R_3Co_4Sn_{13}$ compounds.

TABLE I. Lattice constant a_0 (Å), bulk modulus B (GPa), pressure derivative of bulk modulus B_p, and internal coordinates of Sn2 atoms, obtained after the geometry optimization. Note that the corresponding experimental values are presented in the parentheses.

				Coordinates of Sn2 atom		
Compounds	a_0 (expt.)	B	B_p	x (expt.)	y (expt.)	z (expt.)
$La_3Co_4Sn_{13}$	9.5496 (9.6430[a])	82.57	4.31	0 (0[a])	0.30164 (0.30189[a])	0.15702 (0.15684[a])
$Ce_3Co_4Sn_{13}$	9.4485 (9.6022[a])	105.32	6.40	0 (0[a])	0.30306 (0.30286[a])	0.15681 (0.15688[a])
$Sm_3Co_4Sn_{13}$	9.4200	114.16	9.68	0	0.30488	0.15678
$Gd_3Co_4Sn_{13}$	9.4111 (9.51[b])	127.52	3.97	0	0.30344	0.15789
$Tb_3Co_4Sn_{13}$	9.3958 (9.5072[c])	136.89	8.47	0 (0[c])	0.30380 (0.30488[c])	0.15786 (0.15678[c])

[a]Reference 26.
[b]Reference 28.
[c]Reference 29.

orbit coupling (SOC) effect of R atoms under crystal field, namely, GGA+SOC-type calculation. Furthermore, to improve the description of the strongly correlated $4f$ electrons, we have also introduced the on-site Coulomb energy U correction, the GGA+SOC+U-type calculation.[40] The parameter U was selected as 1.5, 3.0, 5.0, and 8.0 eV for $4f$ electrons of Ce-, Sm-, Gd-, and Tb-based compounds, respectively. In addition, to improve visibility the results of density of states (DOS) have been smoothed using a Gaussian with a width of σ=0.04 eV. Moreover the origin of the energy scale corresponds to the Fermi energy (E_F) in all graphics results.

III. RESULTS AND DISCUSSION

A. Optimized structure and chemical bonding

To obtain the ground-state geometric configuration, the optimization calculation was first carried out at a series of volumes with the relaxation of atomic positions, starting from experimental parameters. The forces on the atoms were calculated, and the atoms were relaxed until the forces had converged to less than 5.0 mRy/a.u. The calculated total energy versus unit-cell volume is fitted with the Birch-Murnaghan equation of state.[41,42] Thus, the equilibrium volume V_0 and lattice constant a_0 are obtained. In Table I, we summarize the results of geometry optimizations of these five intermetallic compounds. The corresponding experimental references in brackets are taken from the values at the room temperature. It is found that the theoretical values of lattice parameters are 1% smaller than the experimental ones on average. This can be explained as the effect of temperature, since this DFT calculation is at the 0 K level. The experimental lattice constant of 9.5810 Å (Ref. 14) of $Ce_3Co_4Sn_{13}$ at 140 K trends toward the theoretical result of 9.4458 Å with the decrease in temperature. From $La_3Co_4Sn_{13}$ to $Tb_3Co_4Sn_{13}$, in addition, the decrease in lattice constants arises from the decrease in atomic radius. In the initial structures, only the Sn2 atoms are not located at the most stable position. The internal coordinates of Sn2 after relaxation are shown in Table I. It is noted that the bulk modulus B increases from the La to Tb compounds, which shows the hardest $Tb_3Co_4Sn_{13}$ and the softest $La_3Co_4Sn_{13}$ among these same-type materials. It was also found from the test that the bulk modulus is strongly dependent on the computational method and the number of selected sample parameters on both sides of experimental lattice constant. Hence, we adopted the GGA-type calculation for La and Gd systems while GGA+U-type calculation for Ce, Sm, and Tb compounds. Moreover to balance the accuracy and calculation load, 21 sample parameters around the experimental lattice constant were selected in this work.

The nearest-neighbor atomic distance, $d_{\text{Co-Sn2}}$, $d_{\text{Co-Sn1}}$, $d_{\text{Sn1-Sn2}}$, $d_{R\text{-Sn2}}$, $d_{R\text{-Co}}$, $d_{R\text{-}R}$, and $d_{\text{Co-Co}}$ are shown in Table II. The bonding length of Co-Sn2 is the shortest in these compounds, $d_{\text{Co-Sn2}} \sim 2.55$ Å. The $d_{R\text{-}R}$ is equal to $d_{\text{Co-Co}}$, which is the longest, 4.698–4.775 Å for five compounds. The $d_{R\text{-Sn2}}$, ~3.3 Å, is larger than $d_{\text{Co-Sn2}}$. Moreover there is a larger distance between Co and Sn1 atoms, ~4.1 Å. The difference in charge density $\Delta\rho$ represents the difference between the crystalline electron density and the superposition of electron densities from the neutral atoms, which qualitatively depicts the bonding interaction of atoms in these compounds. Figure 2 shows the calculated 3D result in the case of $Ce_3Co_4Sn_{13}$. It is visible that there is high charge density between Co and Sn2 atoms, which implies a strong covalent bonding interaction. Only weak bonding interactions exist between Sn1 and Sn2, and R and Sn2 as well as R and Co atoms. Moreover we found that the bonding features among atoms are similar in these five compounds. The variation in charge density mainly comes from the surrounding R ions due to the different $4f$ electronic configurations for La-Tb atoms. So we only present the result of $Ce_3Co_4Sn_{13}$ in Fig. 2. However, the valence states of the components in $R_3Co_4Sn_{13}$ are incompletely known, which is very puzzling in most intermetallics all the while. Interestingly, the research of magnetism and magnetic interaction is a challenge. We start the description of the electronic structures of these compounds in Secs. III B–III E of this paper, where the bonding character and valence states can be also reflected further.

B. $La_3Co_4Sn_{13}$

Figure 3 presents the total DOS of $La_3Co_4Sn_{13}$ unit cell and atomic partial density of states (PDOS). Moreover Fig. 4

TABLE II. The calculated nearest-neighbor atomic distances in each intermetallics (in Å).

	$d_{\text{Co-Sn2}}$	$d_{\text{Co-Sn1}}$	$d_{\text{Sn1-Sn2}}$	$d_{R\text{-Sn2}}$	$d_{R\text{-Co}}$	$d_{R\text{-}R}$	$d_{\text{Co-Co}}$
$La_3Co_4Sn_{13}$	2.594	4.135	3.247	3.397	3.376	4.775	4.775
				3.312			
$Ce_3Co_4Sn_{13}$	2.570	4.090	3.223	3.351	3.340	4.723	4.723
				3.280			
$Sm_3Co_4Sn_{13}$	2.566	4.079	3.229	3.332	3.330	4.710	4.710
				3.274			
$Gd_3Co_4Sn_{13}$	2.557	4.075	3.219	3.341	3.327	4.706	4.706
				3.259			
$Tb_3Co_4Sn_{13}$	2.554	4.069	3.217	3.334	3.322	4.698	4.698
				3.254			

shows the corresponding band structure along high-symmetry directions [$R(0.5,0.5,0.5)$, $\Gamma(0,0,0)$, $X(0.5,0,0)$, $M(0.5,0.5,0)$] in the FBZ. $La_3Co_4Sn_{13}$ exhibits the metallic behavior, and the two bands mixed by Co $3d$ and Sn2 $5p$ cross the E_F, forming a sharp DOS peak. $4f$ empty bands localize around 2.5 eV over the E_F since the electronic configuration is $4f^0 5d^1 6s^2$ in La atom. The $5d$ bands of La are extended with distributing about in 1.0–7.0 eV over the E_F, and a small number of states are occupied by $5d$ electrons below the E_F. La $6s$ electrons also form empty bands which are not observed in the present energy range shown. The Co $3d$ bands mainly contribute in the energy range of $-2.5--0.5$ eV, wider than the empty $4f$ bands. The Co atoms hardly interact with La atoms. Near the E_F, the strong hybridization occurs between Co $3d$ and Sn2 $5p$ states. Under the $Co(Sn2)_6$ trigonal prism environments, the $3d$ orbits of Co are split into d_{z^2}, degenerate $d_{xy}(d_{x^2-y^2})$, and $d_{xz}(d_{yz})$ orbits from low to high energy. The two antibonding bands (respectively, marked by #391 and #392, shown in Fig. 4) mixed by Co $d_{xz}(d_{yz})$ and Sn2 $5p$ cross the E_F to form the complicated Fermi surface (FS). Figure 5 shows the FS sheets of $La_3Co_4Sn_{13}$ in the FBZ. The #391 band with lower energy produces the holelike FS between X and M $\vec{k}$ points, shown in Fig. 5(a). The #392 band with higher-energy forms complex FS, holelike FS along the Γ-R, Γ-X, and Γ-M-X directions (namely, a closed FS surrounding the Γ $\vec{k}$ point), and small electronlike FS around the X $\vec{k}$ point, shown in Fig. 5(b). The FS is mainly constructed by Co $3d$ and Sn $5p$ electrons.

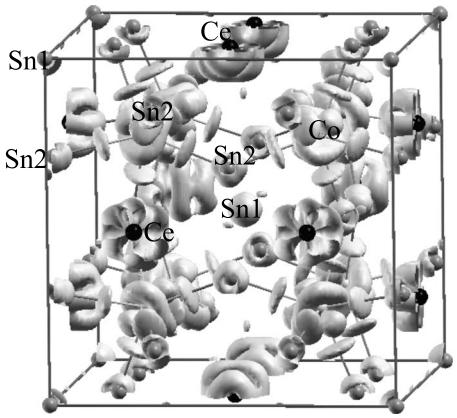

FIG. 2. The 3D maps of difference charge density $\Delta\rho$ for $Ce_3Co_4Sn_{13}$; the isovalue is 0.005. The black ball represents the Ce atom, the gray ball represents Sn atom, while Co atoms at (0.25, 0.25. 0.25) and its equivalent sites are shaded by the charge density. Moreover the (0, 0, 0) and (0.5, 0.5, 0.5) sites are occupied by the Sn1 atoms, the rest of the gray balls correspond to Sn2 atoms.

Assuming the ferromagnetic (FM) ordering with the spin magnetic moment aligning along z axis, the spin-polarized (SP) calculation showed that the net spin is zero, namely, the number of electrons between spin up and spin down is equal. At the same time, the calculation of AFM ordering gave a higher total energy. Table III presents the difference of total energies under NM, FM, and AFM states, which indicates the magnetic ground state of these five compounds. $La_3Co_4Sn_{13}$ is a NM system, consistent with experimental

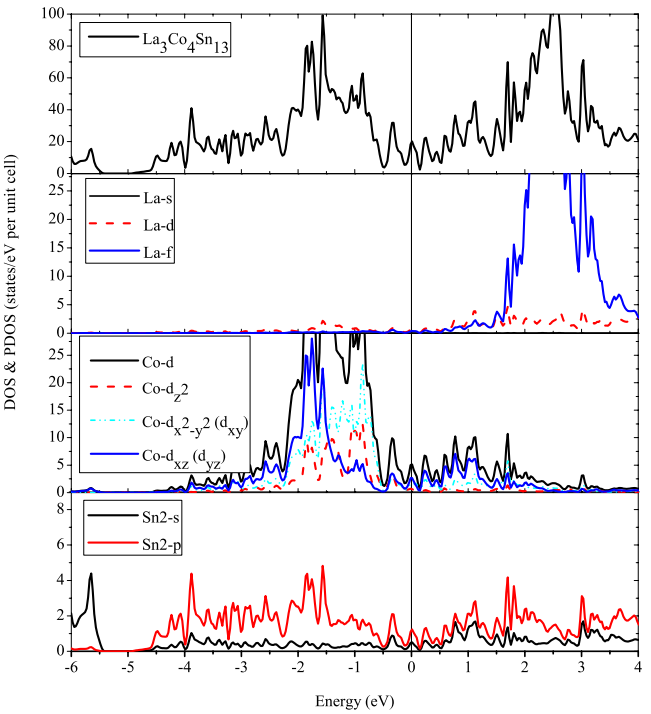

FIG. 3. (Color online) Total and partial densities of states of $La_3Co_4Sn_{13}$ obtained from non-spin-polarized (NSP) calculation.

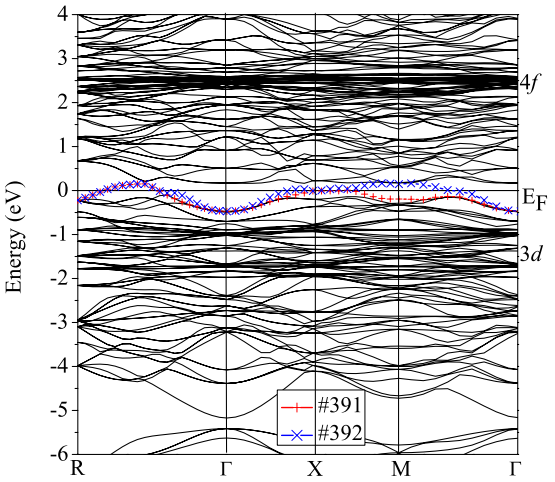

FIG. 4. (Color online) The band structure along the high-symmetry directions of $La_3Co_4Sn_{13}$ obtained from NSP calculation. The dense and flat lines represent $4f$ bands.

result of Pauli paramagnetic metal.[14] However, the difference of total energies of the NSP and SP states is less than 1 meV. There is possibly a strong magnetic instability in $La_3Co_4Sn_{13}$. The sharp DOS peak is localized at the E_F, and the density of states at the Fermi energy (N_{E_F}) reaches about 19.53 states/eV per unit cell. Thus high N_{E_F} not only increases the electron-phonon interaction but also strengthens the spin fluctuations which will suppress superconductivity. So the T_c of this compound is low, ~2 K.[13,14] The superconductivity of $La_3Co_4Sn_{13}$ mainly results from two hybridized bands of Co and Sn2 atoms as mentioned above. $La_3Co_4Sn_{13}$ is similar to the antiperovskite intermetallic $MgCNi_3$ on the superconductivity.[43] Therefore, the superconducting mechanism of $La_3Co_4Sn_{13}$ can be also explained by the conventional BCS theory. Magnetism and superconductivity do not coexist in this compound. In addition, the sharp peak and the high N_{E_F} also indicate a large effective mass coming from p-d coupling. The electronic specific-heat coefficient ~55.64 mJ/(mol K^2) for La compound is bigger than the experimental value of 36 mJ/(mol K^2).[13] In Table IV, we summarize the density of states at the Fermi energy, electronic specific-heat coefficient γ values for all compounds, and magnetic moments of each R atom including the spin and orbital parts as well as the absolute value of their sum.

C. $Ce_3Co_4Sn_{13}$

The total DOS of $Ce_3Co_4Sn_{13}$ unit cell and atomic PDOS obtained from the GGA+SOC+U (U=1.5 eV) calculation

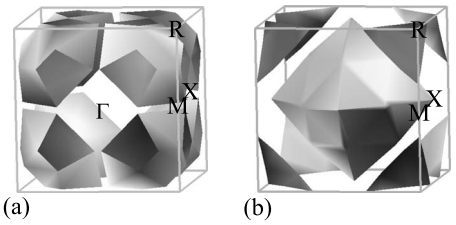

FIG. 5. The Fermi-surface sheets of $La_3Co_4Sn_{13}$ in the first Brillouin zone. The Γ point is at the center of the cubic Brillouin zone, and some other symmetry points are labeled.

are shown in Fig. 6. From the distributions of DOS and PDOS, the electronic state is mainly composed of three parts: Sn $5s$ states at the bottom of energy, p-d hybridization states, and Ce $4f$ states near the E_F. In details, the Sn2 $5s$ electronic states contribute in the energy range of about −10.1−−5.5 eV, while the Sn1 $5s$ electronic states mainly locate in −7.7−−5.5 eV. Moreover the Sn $5p$ (especially Sn2 $5p$) states are very widespread at both sides of the E_F similar to Co $4p$ states. The considerable Co $4s$ states appear at the bottom of the maximum valence bands. Under the crystal field of $Co(Sn2)_6$ trigonal prisms, Co $3d$ orbits are split into d_{z^2}, $d_{x^2-y^2}$, d_{xy}, d_{xz}, and d_{yz} since the SOC effect further lowers the system symmetry. Moreover these $3d$ electronic states mainly cluster below the E_F from −3.0 to −0.5 eV, as well as small number over the E_F. For Ce atoms, the small number of $5p$ states exists below the E_F. The small number of states of Ce $5d$ is occupied, while a large number of states over the E_F is empty. Ce $6s$ states also lie on the E_F with a higher energy than $5d$ electrons. Noticeably, Ce $4f$ electrons occupy the antibonding states near the E_F and form two sharp resonant peaks with a small width of about 0.7 eV. Comparing with the band structures of $La_3Co_4Sn_{13}$, the electron doping (add one f electron) makes the states shift toward lower energy in $Ce_3Co_4Sn_{13}$. The sharp $4f$ peaks are closer to E_F.

There is a strong interaction among the Co $4p$, Sn $5p$, Co $3d$, and Ce $5d$ electrons, forming the p-d hybridization states. The big dispersion of Co $3d$ bands are just induced by the strong hybridization with Sn2 p electrons, since a big space exists between two nearest-neighbor Co atoms, $d_{Co\text{-}Co}$=4.723 while $d_{Co\text{-}Sn2}$=2.570 Å (see Table II). However, these p-d hybridization states are divided by the narrow Ce $4f$ states near the E_F and act as the medium of the interaction of $4f$ electrons. In a word, there is a coupling interaction between $4f$ and c-e (mainly resulted from the p-d hybridization states as well as mixing with a few s states). The interaction between Ce and Co as well as Sn atoms is realized by the coupling of $4f$ and c-e. In addition, very weak

TABLE III. The difference of total energies (meV) under NM, FM, and AFM states for five compounds. For each compound, the energy of the most stable magnetic state is selected as energy reference.

	$La_3Co_4Sn_{13}$	$Ce_3Co_4Sn_{13}$	$Sm_3Co_4Sn_{13}$	$Gd_3Co_4Sn_{13}$	$Tb_3Co_4Sn_{13}$
NM	0.00	8.16	195.64	1462.61	207.49
FM	0.89	0.00	0.00	30.22	0.00
AFM	203.41	273.20	1187.35	0.00	1954.36

TABLE IV. Density of states at the Fermi energy N_{E_F} (states/eV unit cell), electronic specific-heat coefficient [mJ/(mol K^2)], magnetic moment spin M_S, orbital M_L, and absolute value $|M_J|$ (in μ_B) for each R atom. For the La compound, the density of states and specific-heat coefficients are reported for both spins. For the Ce, Sm, Gd, and Tb cases, these figures are reported for each spin direction: spin up/spin down.

		$La_3Co_4Sn_{13}$	$Ce_3Co_4Sn_{13}$	$Sm_3Co_4Sn_{13}$	$Gd_3Co_4Sn_{13}$	$Tb_3Co_4Sn_{13}$
GGA+SOC	N_{E_F}	19.53	17.69/17.58	105.96/14.40	8.27/16.00	4.12/107.00
	γ	55.64	41.69/41.43	249.67/33.93	19.48/37.69	9.70/252.10
	M_S	0.000	0.200	5.410	6.790	5.660
GGA+SOC+U (U=1.5 eV)	N_{E_F}		19.49/10.68	32.20/6.87	7.45/16.44	5.50/26.79
	γ		45.92/25.17	75.87/16.18	17.56/38.75	12.96/63.13
	M_S		0.276	5.241	6.646	5.518
	M_L		−0.396	−1.743	0.135	1.719
	$\|M_J\|$		0.120	3.498	6.781	7.237
GGA+SOC+U (U=3.0 eV)	N_{E_F}		13.06/11.90	21.53/2.86	7.14/16.17	2.37/28.86
	γ		30.77/28.03	50.73/6.73	16.82/38.09	5.58/67.99
	M_S		0.350	5.120	6.641	5.476
	M_L		−0.520	−1.806	0.149	1.848
	$\|M_J\|$		0.170	3.314	6.790	7.324
GGA+SOC+U	N_{E_F}		10.97/14.11	7.80/6.88	4.53/8.56	18.11/19.16
(U=5.0 eV)	γ		25.84/33.24	18.37/16.20	10.68/20.18	42.68/45.15
	M_S		0.929	4.805	6.587	5.113
	M_L		−0.710	−2.612	0.283	2.518
	$\|M_J\|$		0.219	2.193	6.870	7.631
GGA+SOC+U (U=8.0 eV)	N_{E_F}		9.50/14.72	13.52/13.23	5.82/20.43	18.91/14.71
	γ		22.39/34.68	31.86/31.17	13.71/48.14	44.55/34.65
	M_S		0.924	4.857	6.606	5.216
	M_L		−0.794	−1.886	0.203	2.820
	$\|M_J\|$		0.130	1.971	6.809	8.036

hybridization exists between 5s and 5p states of Sn atoms. These interactions are represented in 3D difference charge density shown in Fig. 2.

Figure 7 depicts the energy-band structure of $Ce_3Co_4Sn_{13}$ in the range of −2.0–2.0 eV for spin-up and spin-down channels. It is found that the spin splitting of Ce 4f bands is very small. The spin-down (minority-spin) 4f bands are slightly higher than the spin-up (majority-spin) ones in energy. Obviously, the 4f bands are split into two subbands of $f_{7/2}$ and $f_{5/2}$ due to the SOC effect. Moreover the $f_{5/2}$ DOS peak is about 0.1 eV below the E_F, while the energy of $f_{7/2}$ subband is about 0.40 eV higher than that of $f_{5/2}$ subband. Only the shoulder of $f_{5/2}$ subband crosses the E_F, but the N_{E_F} reaches about 19.49 and 10.68 states/eV per unit cell for majority and minority spins, respectively. The states at the E_F mainly come from the 4f electrons. The very high DOS and flat 4f bands near the E_F indicate a very large electron effective mass, namely, a very small electron mobility in this material. The calculated electronic specific-heat coefficients are about 45.92 and 25.17 mJ/(mol K^2), corresponding to the majority and minority spins, as shown in Table IV; the sum of the coefficients of spin up and spin down is in good agreement with the experimental value of 75 mJ/(mol K^2) at zero temperature.[14] From the band structure, two energy bands (marked by #363 and #364, respectively) cross the E_F in spin-up channel as shown in Fig. 7(a). There are also two bands crossing the E_F in spin-down channel as shown in Fig. 7(b). These two bands construct the complicated FS of $Ce_3Co_4Sn_{13}$. Figures 8(a)–8(d) displays the majority-spin [(a) and (b)] and minority-spin [(c) and (d)] FS sheets in the FBZ. In the majority-spin channel, #363 band induces the complex FS including the holelike and electronlike, while the #364 band forms the electronlike FS between the R and Γ points as well as around the M point (trigonal prisms shape). For the minority spin, the FS sheet seems to be simple. The #363 band forms the electronlike FS along the Γ-X direction and also around the M point, while the #364 band results in the small electronlike FS only around the M point. However, the 4f electrons dominate the FS of $Ce_3Co_4Sn_{13}$ differing from $La_3Co_4Sn_{13}$. In addition, there is a visible gap of minority-spin band structure along the Γ-R and Γ-X directions in the FBZ. Correspondingly, a pseudogap (the density of states is little at one energy point) is found at 0.12 eV below the E_F from the DOS plot of minority spin in Fig. 6. These features indicates a semimetal character of $Ce_3Co_4Sn_{13}$, which is in accordance with the experimental prediction from the entropy and resistivity measurements.[14]

Comparing with $La_3Co_4Sn_{13}$, $Ce_3Co_4Sn_{13}$ is stabilized at the weak FM ground state. The total energy of FM state is 8.16 meV lower than that of the NM state and 273.20 meV lower than that of the AFM state as shown in Table III.

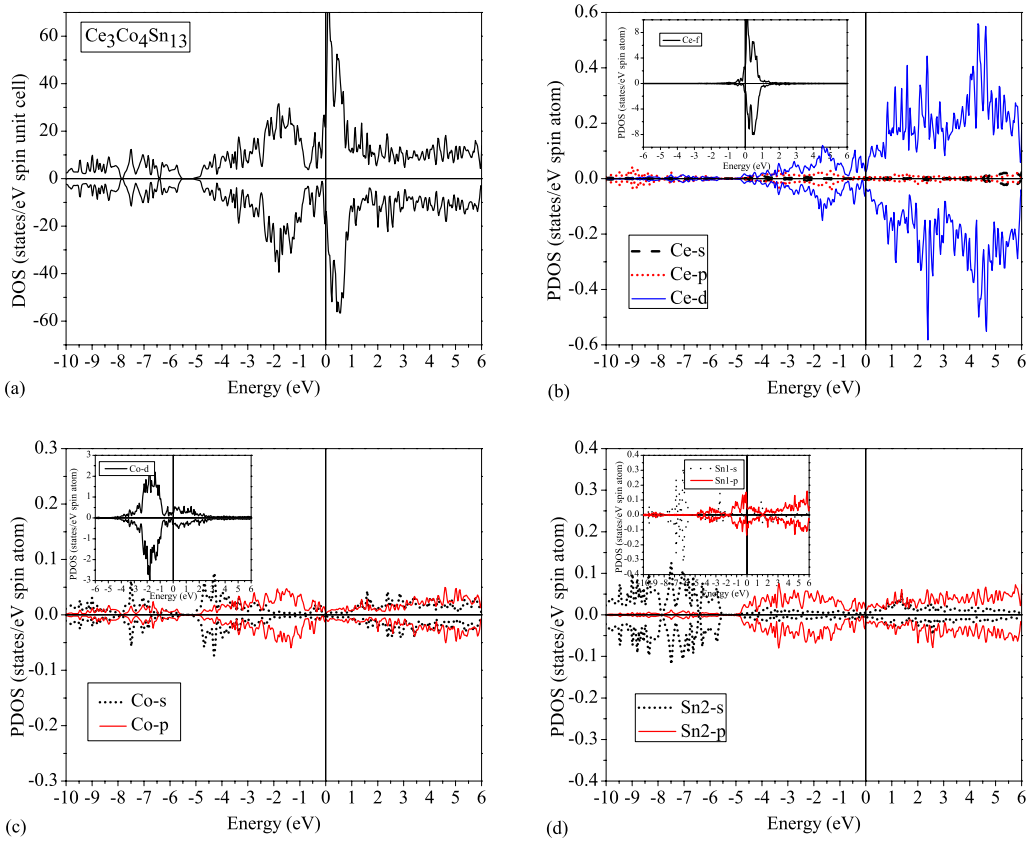

FIG. 6. (Color online) (a) Total density of states of $Ce_3Co_4Sn_{13}$, and atomic partial density of states for (b) cerium, (c) cobalt, and (d) tin obtained from the GGA+SOC+U calculation for $U=1.5$ eV.

Changing the magnetization direction and setting the spin polarization along ⟨001⟩, ⟨110⟩, and ⟨111⟩, respectively, we had not obtained the result of evident magnetocrystalline anisotropy due to the high-symmetry structure. The calculated average spin moment, orbital moment, and total magnetic moment of Ce atom are $0.276\mu_B$, $-0.396\mu_B$, and $0.120\mu_B$, respectively ($U=1.5$ eV in Table IV). Co atom has a very small magnetism with the average spin moment of $-0.043\mu_B$, where the spin direction is opposite to that of the Ce atoms. Sn atom has no magnetism; the average spin moment is only $0.001\mu_B$. In this compound, $3d$ electronic bands do not occur in the visible spin splitting under the strong p-d hybridization. The neglectable magnetic moment suggests a low-spin state ($S\sim 0$) in Co atoms. Hence, the magnetic moment is mainly offered by the Ce $4f$ electrons in $Ce_3Co_4Sn_{13}$.

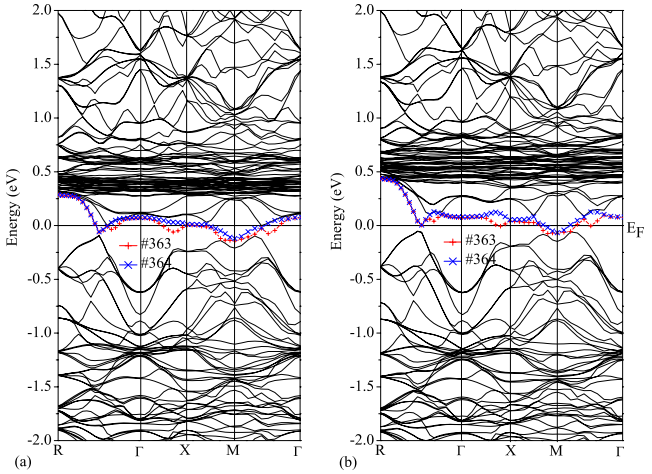

FIG. 7. (Color online) The band structure along the high-symmetry directions of $Ce_3Co_4Sn_{13}$ obtained from the GGA+SOC+U calculation for $U=1.5$ eV. (a) Spin up; (b) spin down. The dense and flat lines represent $4f$ bands.

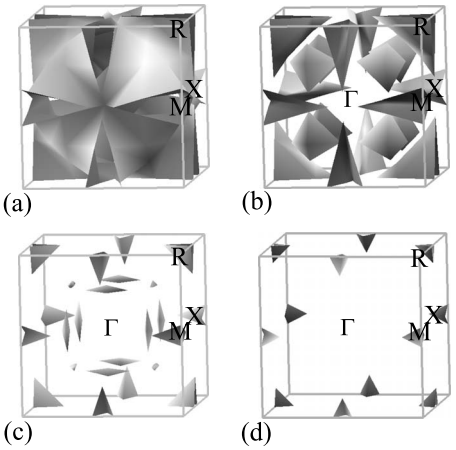

FIG. 8. The Fermi-surface sheets of $Ce_3Co_4Sn_{13}$ in the first Brillouin zone. (a) and (b) correspond to the spin up; (c) and (d) correspond to the spin down. The Γ point is at the center of the cubic Brillouin zone, and some other symmetry points are labeled.

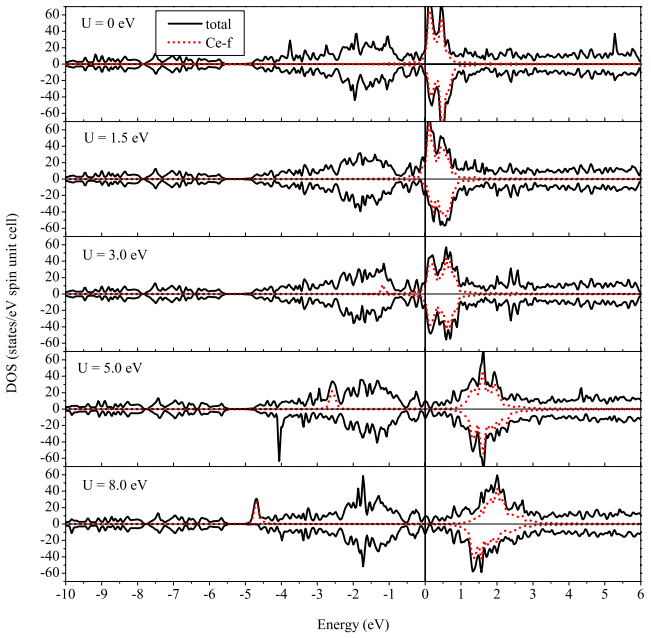

FIG. 9. (Color online) Total and Ce atomic partial densities of states of $Ce_3Co_4Sn_{13}$ dependent on the parameter U (0, 1.5, 3.0, 5.0, and 8.0 eV).

But the magnetism is weak, and the obtained spin moment is still less than the local spin magnetic moment of the single f electron. From the electronic structures, the magnetic moment arises from the spin splitting of the Ce $4f$ band near the E_F. The number of majority-spin f electron is $n_f^{\uparrow} \sim 0.613$, while the number of minority-spin f electron is $n_f^{\downarrow} \sim 0.337$. The $4f$ electrons are approximately in the low-spin state. The coupling interaction of $4f$ and c-e near the E_F results in a strong itinerant feature of the $4f$ electron. Thus, the weak FM ordering is suggested in this material. However, the AFM or only the short-range magnetic order in this compound was indicated by experiments.[13–16] Thus, the losing or reducing magnetic moment of $Ce_3Co_4Sn_{13}$ in experimental measurements is mainly due to the many-body Kondo screening effect or strong spin fluctuations. After considering the spin fluctuations, the NM result is possibly obtained.[44] In addition, the f-electron population ($\sim$0.95) of Ce ions in their MT spheres is closed to 1.0, which implies a Ce^{3+} ion in $Ce_3Co_4Sn_{13}$.

Ce-based compounds are known to challenge the electronic structure method because of the variety of the $4f$ electronic behavior.[45,46] Introducing the on-site Coulomb energy parameter U is regarded as one of the approaches to clearly understand the f electronic nature. In general, the R elements possess a bigger U value such as from 5.0 to 12 eV.[30,45–48] But some calculations also suggested that the results induced by small U parameters (such as 1.5–3.0 eV) fitted with the experiments well.[49,50] In fact, the U value is often variational in different systems. Basing on this and reducing the calculation load, we chose these U values of 1.5, 3.0, 5.0, and 8.0 eV to investigate the correlative intensity of the $4f$ electrons. Figure 9 shows the total DOS of unit cell and PDOS of Ce $4f$ changing with U values. It is noticeable that the spin splitting of $4f$ bands becomes very clear with the increase in the U value. When U is changed from 0.0 to 3.0 eV, the bottom of Ce $4f$ states still crosses the E_F, and the Fermi surface is mainly formed by Ce $4f$ electrons. At $U=1.5$ eV, the electronic states of Ce $4f$ shift toward lower-energy level and begin to occur in the splitting of occupied and unoccupied states. When $U=3.0$ eV, a small local peak of $4f$ states appears at about 1.15 eV below the E_F due to the spin-up band splitting. When $U=5.0$ eV, the $4f$ electronic states are further far away from the E_F, and a completely local peak of $4f$ states is formed at about 2.60 eV below the E_F. Adding U to 8.0 eV, the intensity of this local peak of $4f$ is unchanged but its energy becomes much lower, at about -4.8 eV. From 5.0 to 8.0 eV of U, the N_{E_F} is also decreased, in particular, the $4f$ electrons do not contribute to the Fermi surface.

The spin moment and the absolute value of orbital moment of Ce atoms both increase with the parameter U, shown in Table IV. Until $U=3.0$ eV, the Ce atoms possess increasing itinerant magnetic moment, such as $0.200\mu_B$, $0.276\mu_B$, and $0.350\mu_B$ for $U=0.0$, 1.5, and 3.0 eV, respectively. All these spin moments are less than the local spin moment of one f electron, so $4f$ electrons are in the low-spin or middle-spin state. When $U=5.0$ eV, however, the spin moment of $0.929\mu_B$ is close to that of a single f electron. $4f$ electrons exhibit complete localization and are in high-spin state. While continuously adding U from 5.0 to 8.0 eV, the $4f$ electrons still keep the high-spin and localized characteristics. It indicates that $4f$ electrons gradually transform from the low-spin state to the high-spin state with the increase in the U value. The electronic and magnetic properties of $4f$ electrons occur at a transition from itinerancy to localization while changing U from 3.0 to 5.0 eV. In fact, extracting the U value between 3.0 and 5.0 eV, the calculation showed that $4f$ electrons had become fully local at $U=4.0$ eV. In spite of these transitions, the number of $4f$ electrons of Ce ions is about 1.0 all along in their MT spheres. The Ce^{3+} charge state is favorable and the mixed-valence phenomenon has not been observed in $Ce_3Co_4Sn_{13}$.

Comparing these results with experiments, we know that the $4f$ electron is really itinerant in $Ce_3Co_4Sn_{13}$ due to the strong interaction with c-e. From Table IV, the electronic specific-heat coefficient at $U=1.5$ eV is the one the nearest the experimental value of 75 mJ/(mol K^2).[14] The energy-band structure at this U value also gives out the semimetallic character implied by the entropy and resistivity measurements.[14] Moreover the very weak itinerant magnetism at $U=1.5$ eV indicates that the long-range magnetic ordering may not exist in $Ce_3Co_4Sn_{13}$. On the contrary, this intermetallic compound exhibits a strong local ferromagnetism after $U=4.0$ eV which is quite different from the paramagnetic result in experiments. Meanwhile, the decreasing of N_{E_F} and the losing of $4f$ states at the E_F for higher U situations are not consistent with the electronic properties of heavy fermion systems. Hence, the parameter $U=1.5$ eV can present the result that fits with the experiments well. The correlation effects of $4f$ electrons are not strong in the $Ce_3Co_4Sn_{13}$ system. This kind of weak correlation phenomena of $4f$ electrons have been also observed in $CeRhIn_5$ and $CeCoIn_5$.[49,50] For the intermetallic CeNiSn, the results with $U=5.0$ eV gave a big local magnetic moment of Ce atoms, and the Ce $4f$ electrons formed a local DOS peak about at

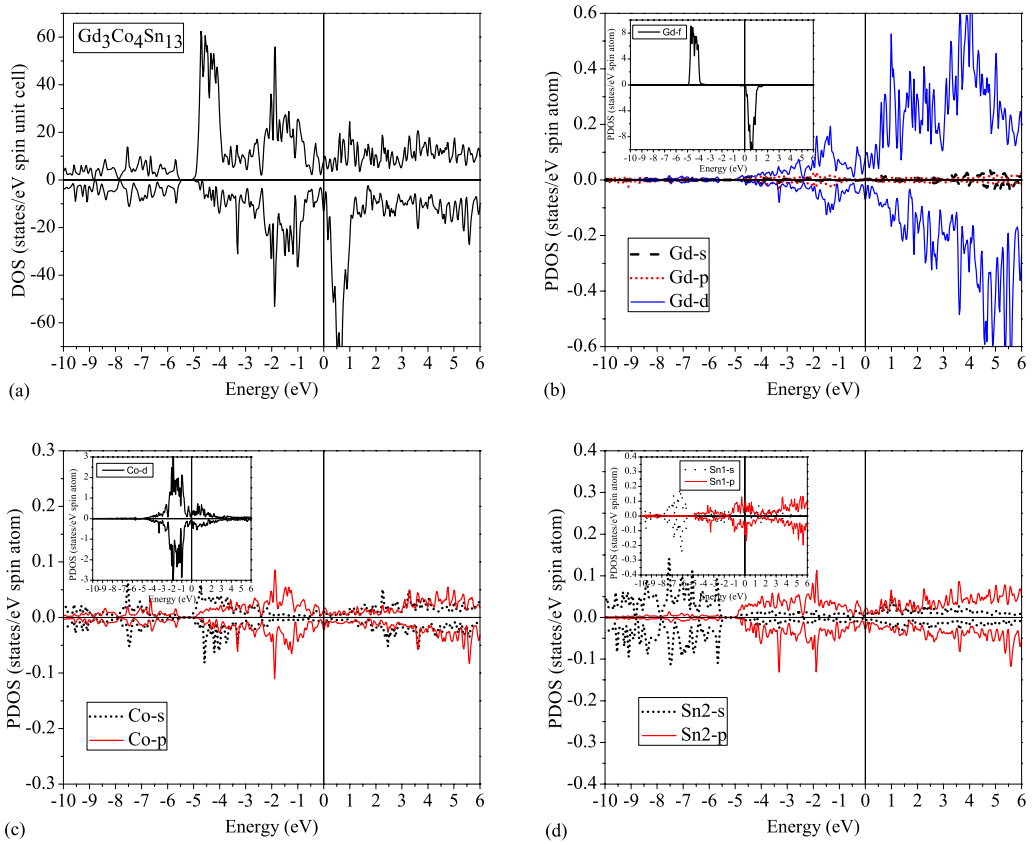

FIG. 10. (Color online) Total and Gd atomic partial densities of states of $Gd_3Co_4Sn_{13}$ obtained from the GGA+SOC (U=0.0 eV) calculations.

1.5 eV below the E_F.[30] However, the CeNiSn does not show magnetic order. Further summarizing some Ce-based compounds, 4f electrons all form very big and local states near the E_F which foreshows the big electronic effective mass or the small mobility, and it is just the reason why they often exhibit the heavy fermion behavior.

D. $Gd_3Co_4Sn_{13}$

$Gd_3Co_4Sn_{13}$ is the case with the half-filled occupancy of 4f orbits in Gd atom. The total and atomic partial densities of states and band structure are shown in Figs. 10 and 11, respectively, obtained from the GGA+SOC (U=0 eV) calculation. It is found that the electronic states of Co and Sn atoms only have slight difference compared with the Ce compound. The main interaction still comes from the hybridization of p-d electrons near the E_F. In the spin-up channel, Gd 4f states are at the bottom of the maximum valence states formed by the p-d hybridization, located around −4.5 eV. The band width is about 0.5 eV; broader DOS peak is observed in Fig. 10 due to the Gaussian broadening effects. While in the spin-down channel, the unoccupied 4f states appear in the range of about 0–1.0 eV. The majority-spin states of 4f electrons interact with the minority-spin states by the p-d hybridization bands. Comparing with the Ce analog, the occupied 4f states are far below the E_F with the small interaction between 4f and c-e in $Gd_3Co_4Sn_{13}$. This estimated effective exchange interaction is only 10 meV.[27] Thus, 4f states are fully local and seem to be the impurity electronic energy level in band structure shown in Fig. 11. The p-d hybridization bands mainly contribute to the Fermi surface. The #403 and #404 bands cross the E_F in the majority spin, while the #361 and #362 bands do in the minority spin. Figures 12(a)–12(d) display the majority-spin [(a) and (b)] and minority-spin [(c) and (d)] FS sheets in the FBZ. Partly

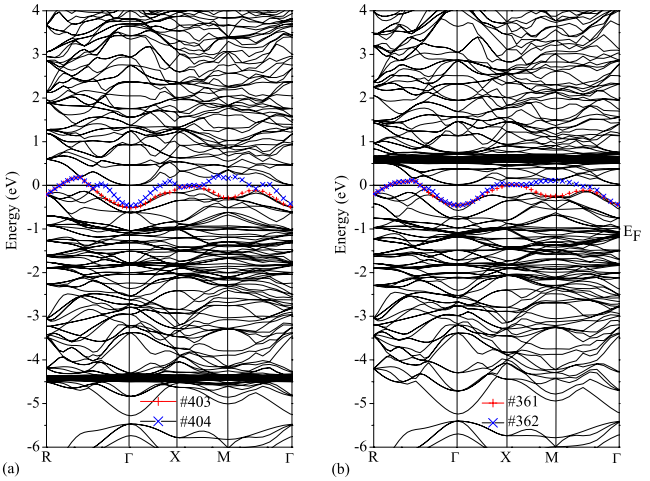

FIG. 11. (Color online) The band structure along the high-symmetry directions of $Gd_3Co_4Sn_{13}$ obtained from the GGA+SOC calculation. (a) Spin up; (b) spin down. The dense and flat lines represent 4f bands.

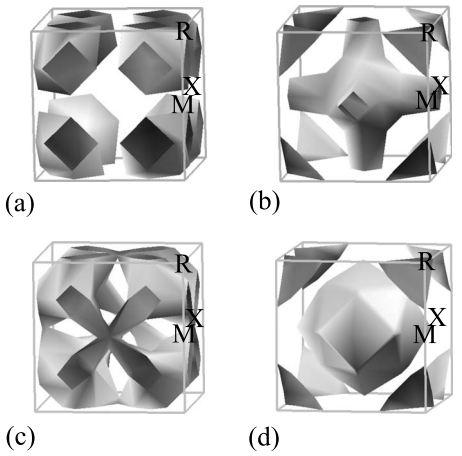

FIG. 12. The Fermi-surface sheets of $Gd_3Co_4Sn_{13}$ in the first Brillouin zone. (a) and (b) correspond to the spin up; (c) and (d) correspond to the spin down. The Γ point is at the center of the cubic Brillouin zone, and some other symmetry points are labeled.

FS characters [Figs. 12(a) and 12(d)] are similar to those of $La_3Co_4Sn_{13}$. $Gd_3Co_4Sn_{13}$ displays the metallic character but the DOS at the E_F is somewhat smaller. The calculated N_{E_F} shown in Table IV are about 8.27 and 16.00 states/eV per unit cell for the majority and minority spins. The electronic specific-heat coefficients are about 19.48 and 37.69 mJ/(mol K^2) for the majority and minority spins, respectively.

Plus the parameter U, the electronic structures of $Gd_3Co_4Sn_{13}$ are almost unchanged. The position of the $4f$ electronic energy level is independent on the parameter U. This similar phenomenon was also observed in the Gd-doped GaN magnetic semiconductor.[51] It can be explained by the electronic configuration of $4f^75d^16s^2$ in Gd atoms. Seven f electrons occupy the spin-up bands and exhibit the high-spin Gd^{3+} state ($S\sim 7/2$), which obeys Hund's rule. The U parameter does not influence the $4f$ electronic states. Setting the AFM spin ordering, as shown in Table III, the lower total energy is obtained, which means that $Gd_3Co_4Sn_{13}$ has AFM ground state. Differing from Ce compound, therefore, the Coulomb energy U cannot lead the variations in band and spin splittings in local antiferromagnetic $Gd_3Co_4Sn_{13}$. The calculated spin magnetic moment of $6.790\mu_B$ of Gd approaches the fully local $7.0\mu_B$. Co and Sn atoms antiferromagnetically couple with Gd. Moreover the spin moment of Gd is unchanged with the parameter U. Nonzero orbital moment is obtained owing to the incomplete splitting of $4f$ orbits induced by the crystal-field effects. In addition, from the electronic structures of Gd ion, a Gd^{3+} valence state is preferred in the $Gd_3Co_4Sn_{13}$ system.

E. $Sm_3Co_4Sn_{13}$ and $Tb_3Co_4Sn_{13}$

From the results above, the $4f$ electron is itinerant in $Ce_3Co_4Sn_{13}$ while it is localized in $Gd_3Co_4Sn_{13}$. For Sm atom ($4f^65d^06s^2$), there are six $4f$ electrons that are only slightly less than the half-filled Gd. The total DOS of $Sm_3Co_4Sn_{13}$ and PDOS of $4f$ electrons are shown in Fig. 13, obtained from the GGA+SOC+U (U=0,3.0 eV) calculations. Without the U correction, the Sm $4f$ states form three very sharp peaks. The E_F lies on the peak with the highest energy. The $4f$ states strongly couple with the c-e, which results in the very large N_{E_F} and electronic specific-heat coefficient, ~105.96 states/eV per unit cell and ~249.67 mJ/(mol K^2) (seen in Table IV) in the majority-spin channel. These are implications of strong electronic correlation. On the contrary, the E_F is near a pseudogap in the minority-spin channel, and the minority-spin $4f$ states are fully emptied.

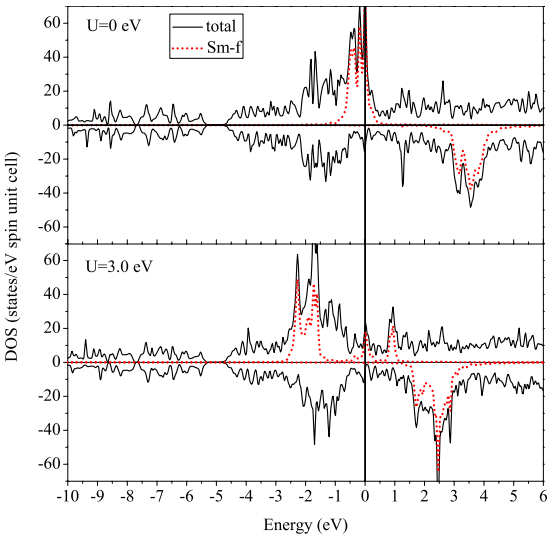

FIG. 13. (Color online) Total and Sm atomic partial densities of states of $Sm_3Co_4Sn_{13}$ obtained from the GGA+SOC and GGA+SOC+U (U=3.0 eV) calculations.

Introducing the U parameter, the $4f$ electronic states gradually shift toward the lower energy with the increase in the U value. When U=3.0 eV, the band splitting occurs. Most majority-spin $4f$ states are located at the bottom of the Co $3d$ states, about −2.5−−1.5 eV, and there is a strong bonding hybridization between $4f$ and $3d$ states. A few spin-up $4f$ electrons additionally occupy the antibonding states near the E_F. Noticeably, two small local peaks of the $4f$ states appear at the E_F and 1.0 eV in the majority-spin channel. The fully $4f$ empty states distribute in the range of about 1.5–3.0 eV in the minority-spin channel. As a result, the N_{E_F} becomes very small, especially only about 2.86 states/eV per unit cell for the minority-spin case. The E_F is much nearer the pseudogap in the spin-down channel. The obvious semimetallic character is also observed in this material. When adding the U value, such as the Ce compound, the splitting of the majority-spin $4f$ bands further becomes larger. But the hybridization between the f and d electrons becomes weak. The localized character of $4f$ electrons is much clearer.

Comparing the total energies under NM, FM, and AFM states shown in Table III, we found that $Sm_3Co_4Sn_{13}$ is ferromagnetic. The calculated magnetic moment is 5.12 (spin), −1.806 (orbital), and 3.314 (absolute value of sum) μ_B at U=3.0 eV, respectively. The electronic structures and magnetic moment suggest a Sm^{3+} charge state. About one of the six f electrons in Sm atom is bonding. The rest of the f

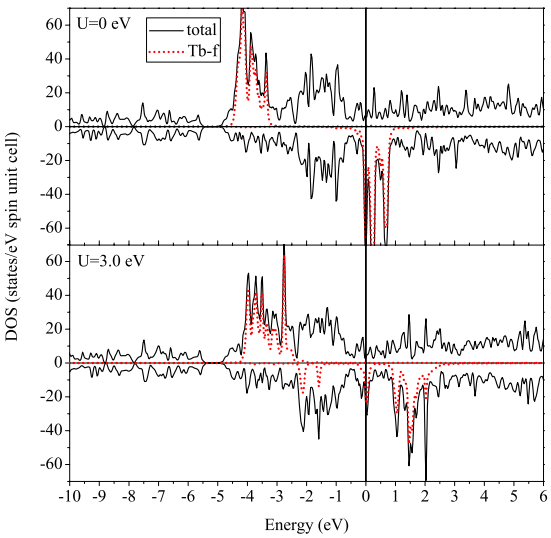

FIG. 14. (Color online) Total and Tb atomic partial densities of states of $Tb_3Co_4Sn_{13}$ obtained from the GGA+SOC and GGA +SOC+U (U=3.0 eV) calculations.

electrons are at the high-spin state ($S\sim 5/2$). However, the $4f$-electron population of Sm ion in their MT spheres varies with the U values. From the calculation of GGA+SOC(U =0 eV), the numbers of the $4f$ electron are $n_f^{\uparrow}\sim 5.454$ and $n_f^{\downarrow}\sim 0.044$, and also the spin magnetic moment is about $5.410\mu_B$. These suggest an intermediate charge state for Sm between Sm^{2+} and Sm^{3+} without introducing the on-site Coulomb energy U. It is concluded that $4f$ electrons are partly localized and partly itinerant in this material.

Contrary to Sm and Gd, $4f$ electrons are more than half filled in Tb atoms ($4f^9 5d^0 6s^2$). From the total DOS of $Tb_3Co_4Sn_{13}$ and PDOS of Tb $4f$ shown in Fig. 14, the majority-spin $4f$ states contribute in the range of about −4.5−−3.0 eV at the end of the Co $3d$ states. Seven spin-up f electrons are completely occupied and exhibit the fully localization. In the minority-spin channel, the E_F crosses the bottom of the $4f$ states, resulting in a very high N_{E_F} (~107.00 states/eV per unit cell for U=0 eV). There is a strong-coupling interaction between the spin-up $4f$ and c-e so that the $4f$ electrons display the itinerancy. However, the very small DOS at the E_F (~4.12 states/eV per unit cell for U=0 eV) is in the majority-spin channel. These features show the possible semimetallic behavior in this material. After adding the U parameter, the spin-down N_{E_F} decreases to 28.86 states/eV per unit cell for U=3.0 eV due to the obvious band splitting. Two local peaks appear below the E_F, at about −2.1 and −1.5 eV.

The ferromagnetism is suggested in this Tb material. The calculated magnetic moments are 5.476 (of spin), 1.719 (orbital), and 7.324 (sum of spin and orbital) μ_B at U=3.0 eV, respectively. The majority-spin and minority-spin electrons are $n_f^{\uparrow}\sim 6.813$ and $n_f^{\downarrow}\sim 1.337$. In spite of departure from high-spin state, the f-electron population of Tb ions in their MT spheres varies very little, which is nearly a constant value of 8.15 in our calculation; Tb ions tend to display trivalent charge state in $Tb_3Co_4Sn_{13}$.

F. Magnetic interaction

As mentioned above, the investigation shows that TM atoms hardly possess a magnetic moment in these series. Examining the crystal structural and electronic properties, we suggest that high symmetric Co-Sn2 structure and strong covalent hybridization make the magnetic moment of Co atom approach zero, which is different from those TM-rich systems, such as $La_6Co_{13}Sn$ (Ref. 22) and RCo_3Sn (R=Y and Gd-Yb).[23] Hence, the magnetism is mainly contributed by the R atoms in these intermetallic compounds. With regard to the magnetic interaction of R atoms, the Hill criteria[52] for magnetic order do not apply in the $Ce_3Co_4Sn_{13}$ compound; the Ce-Ce distance of 4.723 Å is larger than the critical distance of 3.4 Å. $Ce_3Co_4Sn_{13}$ is a weak FM in this calculation but paramagnetic in experiments. Introducing the U parameter, the spin splitting becomes larger due to the splitting of $4f$ bands in the Ce compound. However, the AFM order exists in the intermetallic $Gd_3Co_4Sn_{13}$ in which the splitting of band and spin do not appear plus U energy. For $Sm_3Co_4Sn_{13}$ and $Tb_3Co_4Sn_{13}$, the FM ground states are obtained, $4f$ electrons synchronously hold localization and itinerancy, which may need more experiments to sustain this result. In addition, comparing with the R atoms, the spin magnetic moments of Co atoms are negative, though the Co magnetic moment is negligible in these compounds. For f electrons in different atoms, the direct interaction among them is weak. The magnetic interaction of R atoms is realized by the coupling with c-e.

The magnetic transition can be described qualitatively by the one-dimensional Kondo lattice mode of Doniach,[53] where the competition between RKKY interaction and Kondo spin-compensation mechanism determines the magnetic ground state. The AFM interaction is expressed as

$$H_{\text{eff}} = J_{cf}\vec{S}_c\vec{S}_f. \tag{1}$$

Here, $\vec{S}_c$ and $\vec{S}_f$ represent the spin of c-e and local f electron. Moreover the coupling parameter J_{cf} is written as

$$J_{cf} = \frac{V^2}{-E_f} + \frac{1}{E_f + U}, \tag{2}$$

where E_F is set to zero, V is the hybridization matrix element between c-e and f, and E_f corresponds to the energy of f electrons. In Kondo lattice, on one hand, the coupling J_{cf} of c-e and f can result in the Kondo effect which screens the magnetic moment of f electrons and makes the system behave as paramagnetic. On the other hand, the local magnetic moment also brings the RKKY interaction by polarizing c-e,

$$J_{\text{RKKY}}(r) \sim -J_{cf}^2 N_{E_F} \frac{\cos(2k_F r)}{|k_F r|^3}, \tag{3}$$

which strengthens the coupling of local moments so that the magnetic ordering ground state is stabilized. The energy scale of the former is $T_K = De^{-1/2J_{cf}N_{E_F}}$ and that of the latter is $T_{\text{RKKY}} = J_{cf}^2 N_{E_F}$ where D is the width of the c-e band. When $J_{cf}N_{E_F}$ is very small, $T_{\text{RKKY}} \gg T_K$, RKKY interaction dominates and the AFM ground state forms in the system. The local magnetic moment is stabilized, and the f electron does

not contribute to the FS, such as $Gd_3Co_4Sn_{13}$. When $J_{cf}N_{E_F}$ is very big, on the contrary, $T_K \gg T_{RKKY}$, the Kondo effect is primary. The Kondo single state is formed at low temperature. The f electron does not possess the local behavior, forming the reorganized f band with the width of $\sim T_K$. The strong itinerant character is observed, corresponding to the FS that includes the contribution of f and c-e, such as $Ce_3Co_4Sn_{13}$. However, $Ce_3Co_4Sn_{13}$ is near the magnetic QCP in $Ce_3Co_4Sn_{13}$.[15] The excitation of quasiparticle is very complicated and exhibits the non-Fermi-liquid behavior. The f electronic feature is not completely clear.

IV. SUMMARY

We have investigated the chemical bonding, electronic structures, and magnetic properties of $R_3Co_4Sn_{13}$ (R=La, Ce, Sm, Gd, and Tb) intermetallic compounds by the use of the FPLAPW method within the framework of DFT with GGA and GGA+U techniques. After a full geometry optimization of crystal structure, we analyzed the interatomic interaction and calculated the charge density, total and partial density of states, and band structure along high-symmetry directions, as well as the Fermi-surface features. Introducing the on-site Coulomb energy parameter U, moreover, the 4f electronic correlation has been studied.

In $La_3Co_4Sn_{13}$, the superconductivity is related with the hybridization bands of Co 3d and Sn 5p electrons. The competition between superconductivity and magnetism exists in this material. $Ce_3Co_4Sn_{13}$ has a weak FM ground states for $U \leq 3.0$ eV, but the paramagnetic result in experiments implies strong spin fluctuations in this material. The 4f electron is itinerant and strongly couples with conduction electrons in $Ce_3Co_4Sn_{13}$. There is a transition from itinerancy to localization with the increase in the U value in this compound. The low-spin state gradually changes into high-spin state simultaneously. But the correlation of 4f electrons is not strong in this material. Moreover the metallic behavior with semimetallic character is also suggested. 4f electrons are fully local and their energy position is unchanged with the U value in $Gd_3Co_4Sn_{13}$. The local f bands hardly couple with conduction electrons. The AFM interaction exists in this compound. f electrons are partly localized and itinerant in $Sm_3Co_4Sn_{13}$ and $Tb_3Co_4Sn_{13}$. 4f electrons are a moderate correlation in these two compounds. Though this series exhibits a different low-temperature behavior, the f-electron population of R ions in their MT spheres varies very little, indicating the trivalent R ions in these compounds. The magnetic moment mainly results from the R ions in these compounds. TM and Sn atoms hardly possess magnetism due to the $Co(Sn)_6$ sublattice, strong covalent interaction between them.

The f electrons in heavy fermion compounds usually experience a crossover from behaving as a localized single impurity at high temperature to forming the itinerant heavy fermion quasiparticle band at low temperate due to the coherent Kondo interaction. Moreover the dynamic spin fluctuation cannot be taken into account in this calculation. Although the on-site Coulomb energy U is introduced, both GGA and GGA+U are static mean-field approximation and cannot capture these features. So some results are different from the experiments. However, our motivation of the study is to understand the electronic structural characteristics and how much of the localization of f electrons is affected by a reasonable choice of U parameter, provided that the correlation effect of f electrons cannot be neglected in these systems.

ACKNOWLEDGMENTS

The authors would like to thank W. H. Wang for help in writing and also J. L. Wang and Y. L. Li for their meaningful discussion. This work was supported by the National Nature Science Foundation of China (Grants No. 20573113, No. 20731006, No. 20821061, and No. 20825104).

*ghzhong_2007@163.com
†mjg@fjirsm.ac.cn

[1] G. R. Stewart, Rev. Mod. Phys. **56**, 755 (1984); **73**, 797 (2001).
[2] R. V. Skolozdra, in *Handbook on the Physics and Chemistry of Rare Earths*, edited by K. A. Gschneidner and L. Eyringvol (Elsevier, Netherlands, 1997), Vol. 24, p. 399.
[3] A. Ślebarski, A. Jezierski, A. Zygmunt, S. Mähl, M. Neumann, and G. Borstel, Phys. Rev. B **54**, 13551 (1996).
[4] D. Kaczorowski, A. Leithe-Jasper, P. Rogl, H. Flandorfer, T. Cichorek, R. Pietri, and B. Andraka, Phys. Rev. B **60**, 422 (1999).
[5] K. Katoh, G. Terui, Y. Niide, H. Aoki, and A. Ochiai, Physica B **259-261**, 161 (1999).
[6] O. Trovarelli, C. Geibel, R. Cardoso, S. Mederle, R. Borth, B. Buschinger, F. M. Grosche, Y. Grin, G. Sparn, and F. Steglich, Phys. Rev. B **61**, 9467 (2000).
[7] R. Pietri, B. Andraka, D. Kaczorowski, A. Leithe-Jasper, and P. Rogl, Phys. Rev. B **61**, 12169 (2000).
[8] B. Andraka, R. Pietri, D. Kaczorowski, A. Leithe-Jasper, and P. Rogl, J. Appl. Phys. **87**, 5149 (2000).
[9] H. Sato, T. Fukuhara, S. Iwakawa, Y. Aoki, I. Sakamoto, S. Takayanagi, and N. Wada, Physica B **186-188**, 630 (1993).
[10] S. Takayanagi, H. Sato, T. Fukuhara, and N. Wada, Physica B **199-200**, 49 (1994).
[11] C. Nagoshi, H. Sugawara, Y. Aoki, S. Sakai, M. Kohgi, H. Sato, T. Onimaru, and T. Sakakibara, Physica B **359-361**, 248 (2005).
[12] M. F. Hundley, J. L. Sarrao, J. D. Thompson, R. Movshovich, M. Jaime, C. Petrovic, and Z. Fisk, Phys. Rev. B **65**, 024401 (2001).
[13] C. Israel, E. M. Bittar, O. E. Agüero, R. R. Urbano, C. Rettori, I. Torriani, P. G. Pagliuso, N. O. Moreno, J. D. Thompson, M. F. Hundley, J. L. Sarrao, and H. A. Borges, Physica B **359-361**, 251 (2005).
[14] E. L. Thomas, H. O. Lee, A. N. Bankston, S. MaQuilon, P. Klavins, M. Moldovan, D. P. Young, Z. Fisk, and J. Y. Chan, J. Solid State Chem. **179**, 1642 (2006).

[15] A. L. Cornelius, A. D. Christianson, J. L. Lawrence, V. Fritsch, E. D. Bauer, J. L. Sarrao, J. D. Thompson, and P. G. Pagliuso, Physica B **378-380**, 113 (2006).
[16] A. D. Christianson, J. S. Gardner, H. J. Kang, J.-H. Chung, S. Bobev, J. L. Sarrao, and J. M. Lawrence, J. Magn. Magn. Mater. **310**, 266 (2007).
[17] C. D. Routsi, J. K. Yakinthos, and H. Gamari-Seale, J. Magn. Magn. Mater. **117**, 79 (1992).
[18] F. Canepa and S. Cirafici, J. Alloys Compd. **232**, 71 (1996).
[19] J. L. Hodeau, J. Chenavas, M. Marezio, and J. P. Remeika, Solid State Commun. **36**, 839 (1980).
[20] J. P. Remeika, G. P. Espinosa, A. S. Cooper, H. Barz, J. M. Rowell, D. B. McWhan, J. M. Vandenberg, D. E. Moncton, Z. Fisk, L. D. Woolf, H. C. Hamaker, M. B. Maple, G. Shirane, and W. Thomlinson, Solid State Commun. **34**, 923 (1980).
[21] Y. Aoki, T. Fukuhara, H. Sugawara, and H. Sato, J. Phys. Soc. Jpn. **65**, 1005 (1996).
[22] F. Weitzer, A. Leithe-Jasper, P. Rogl, K. Hiebl, H. Noël, G. Wiesinger, and W. Steiner, J. Solid State Chem. **104**, 368 (1993).
[23] R. V. Skolozdra, *Stannides of Rare Earth and Transition Metals* (Svit, Lviv, Ukraine, 1993).
[24] M. Kurisu, R. Hara, G. Nakamoto, Y. Andoh, S. Kawano, and D. Scmitt, Physica B **312-313**, 861 (2002).
[25] B. Chevalier, F. Fourgeot, L. Fournès, P. Gravereau, G. Le Caër, and J. Etourneau, Physica B **226**, 283 (1996).
[26] R. V. Skolozdra, I. V. Yasnitskaya, O. E. Koretskaya, and L. G. Akselīrud, Dopov. Akad. Nauk Ukr. RSR, Ser. B **6**, 42 (1983).
[27] M. A. Pires, L. M. Ferreira, J. G. S. Duque, R. R. Urbano, O. Agüero, I. Torriani, C. Rettori, E. M. Bittar, and P. G. Pagliusoa, J. Appl. Phys. **99**, 08J311 (2006).
[28] X. W. Lei and J. G. Mao (unpublished).
[29] C. Nagoshi, R. Yamamoto, K. Kuwahara, H. Sagayama, D. Kawana, M. Kohgi, H. Sugawara, Y. Aoki, H. Sato, T. Yokoo, and M. Arai, J. Phys. Soc. Jpn. **75**, 044710 (2006).
[30] Andrea Aburto and Emilio Orgaz, Phys. Rev. B **75**, 045130 (2007).
[31] B. Bochu, M. N. Deschizeaux, J. C. Joubert, A. Collomb, J. Chenavas, and M. Marezio, J. Solid State Chem. **29**, 291 (1979).
[32] M. A. Subramanian, W. J. Marshall, T. G. Calvarese, and A. W. Sleight, J. Phys. Chem. Solids **64**, 1569 (2003).
[33] P. Blaha, K. Schwarz, G. K. H. Madsen, D. Kvasnicka, and J. Luitz, in *WIEN2k: An Augmented Plane Wave+Local Orbitals Program for Calculating Crystal Properties*, edited by K. Schwarz (Technische Universität Wien, Austria, 2001).
[34] G. K. H. Madsen, P. Blaha, K. Schwarz, E. Sjöstedt, and L. Nordström, Phys. Rev. B **64**, 195134 (2001).
[35] K. Schwarz, P. Blaha, and G. K. H. Madsen, Comput. Phys. Commun. **147**, 71 (2002).
[36] Z. G. Wu and R. E. Cohen, Phys. Rev. B **73**, 235116 (2006).
[37] P. E. Blöchl, O. Jepsen, and O. K. Andersen, Phys. Rev. B **49**, 16223 (1994).
[38] H. J. Monkhorst and J. P. Pack, Phys. Rev. B **13**, 5188 (1976).
[39] D. D. Koelling and B. N. Harmon, J. Phys. C **10**, 3107 (1977).
[40] V. I. Anisimov, J. Zaanen, and O. K. Andersen, Phys. Rev. B **44**, 943 (1991).
[41] F. D. Murnaghan, Proc. Natl. Acad. Sci. U.S.A. **30**, 244 (1944).
[42] F. Birch, Phys. Rev. **71**, 809 (1947).
[43] G. H. Zhong, J. L. Wang, Z. Zeng, X. H. Zheng, and H. Q. Lin, J. Appl. Phys. **101**, 09G520 (2007).
[44] A. Aguayo, I. I. Mazin, and D. J. Singh, Phys. Rev. Lett. **92**, 147201 (2004).
[45] S. Fabris, S. de Gironcoli, S. Baroni, G. Vicario, and G. Balducci, Phys. Rev. B **71**, 041102(R) (2005).
[46] G. Kresse, P. Blaha, J. L. F. Da Silva, and M. V. Ganduglia-Pirovano, Phys. Rev. B **72**, 237101 (2005).
[47] J. F. Herbst, R. E. Watson, and J. W. Wilkins, Phys. Rev. B **17**, 3089 (1978).
[48] P. Larson, W. R. L. Lambrecht, A. Chantis, and M. van Schilfgaarde, Phys. Rev. B **75**, 045114 (2007).
[49] J. L. Wang, Z. Zeng, Q. Q. Zheng, and H. Q. Lin, J. Appl. Phys. **93**, 6891 (2003).
[50] Y. Xu, J. L. Wang, and Z. Zeng, Chin. Phys. Lett. **22**, 460 (2005).
[51] G. H. Zhong, J. L. Wang, and Z. Zeng, J. Phys.: Condens. Matter **20**, 295221 (2008).
[52] H. H. Hill, Nucl. Metall. **17**, 2 (1970).
[53] S. Doniach, Physica B & C **91**, 231 (1977).